IEEE Journal of Microwaves

Received 4 June 2022; revised 6 August 2022 and 14 November 2022; accepted 30 November 2022. Date of publication 19 December 2022; date of current version 6 January 2023.

Digital Object Identifier 10.1109/JMW.2022.3226878

A Novel Design Methodology to Realize a Single Byte Chipless RFID Tag by Loading a Square Open-Loop Resonator With Micro-Metallic Cells

MUHAMMAD NOMAN [1], USMAN A. HAIDER[1], ANAS M. HASHMI[2], HIDAYAT ULLAH [1], ALI I. NAJAM[3], AND FAROOQ A. TAHIR [1] (Senior Member, IEEE)

(Regular Paper)

[1]School of Electrical Engineering and Computer Science, National University of Sciences and Technology, Islamabad 44000, Pakistan
[2]Department of Electrical and Electronic Engineering, University of Jeddah, Jeddah 23218, Saudi Arabia
[3]National Electronics Complex of Pakistan, Islamabad 44000, Pakistan

CORRESPONDING AUTHOR: Farooq A. Tahir (e-mail: farooq.tahir@seecs.edu.pk).

This work was supported by the Higher Education Commission of Pakistan though the National Research Program for Universities under Project 10038/Federal/NRPU/R&D/HEC/2017.

ABSTRACT In this paper, a unique structural design methodology for chipless radio-frequency identification (RFID) tags in frequency domain is presented. The tag geometry is developed by loading an open-loop resonator with micro-metallic-cells (MMC). The realization give rise to a checkerboard resonator type with electromagnetic signatures in its radar cross section that are extremely efficient to manipulate. The resonators layout is distributed on either side of a Rogers substrate to double its coding density. The proposed chipless RFID tag has a memory of 8-bits in total. The operating band of the tag is 6.5-10.5 GHz. The tag has a high bit coding density of 10.94 bits/cm^2 and spectral efficiency of 2 bits/GHz. The tag has a very compact size of 17.4 $\times$ 4.2 mm^2. The simple structuring methodology and efficient resonators layout will give RFID system designers the flexibility to apply the proposed tag in a wide range of modern applications.

INDEX TERMS Chipless radio frequency identification (CRFID), frequency-domain (FD), miniaturization, open-loop, radar cross section (RCS), resonators, tag.

I. INTRODUCTION

Rapid surge in progression of RFID technology has brought great attention towards chipless tags in the recent years. RFID is a wireless technology that is essentially used for automated identification of objects by using radio frequency (RF) waves [1]. A conventional RFID system consists of two integral parts, 1) RFID tag and 2) RFID reader [2]. The tag of a conventional RFID system contains a silicon integrated chip (IC) which is composed of microprocessor and a memory. The tag is attached to an object storing information about that object. An RFID reader on the other hand is used to communicate with the tag at a distance [3]. The certain very crucial limitations of conventional chip-based RFID tags include the use of silicon IC, on-board antennas, large size and high cost [4]. The 90% cost of the conventional tag lies with the on-board IC [4]. The technology of chipless RFID (CRFID) tag is being seen as a potential replacement of conventional chip-based tags improving many of its limitations.

CRFID system is being proposed as a substitute of conventional RFID system that will use electromagnetic (EM) signatures instead, which effectively eliminates the use of expensive on-board electronics required for a chip-based tag. Other features of CRFIDs include low cost of manufacturing, longer life, compactness, direct printability, physical robustness, long read range, no very strict line-of-sight (LOS) requirement, [5]. These advantages allow CRFID tags to be used in many exciting applications such as internet of things (IoT) [6], classified document security [7], item level tagging,

sensing, environment monitoring, medical diagnosis [8], shipment tracking and warehouse inventory control [9].

Based on the design method, CRFID tags can be classified into two main categories: 1) circuit-based and 2) fully-passive. Circuit-based tags consist of microwave circuitry integrated with transmit-receive antennas. The microwave circuitry has transmission lines and resonators to encode the data, whereas the antennas are used for transmitting and receiving the EM waves [13], [14], [15]. On the other hand, fully-passive tags do not have any kind of active microwave circuitry. The data encoding is embedded in the RCS signature of the tag. These tags, therefore, consist of only resonating structures. Consequently, fully-passive tags are comparatively more compact and have higher code densities [10], [11], [12]. The information stored on a CRFID tag can be decoded by using either frequency domain (FD) or time domain (TD) techniques. Several chipless tags employing the above techniques have been recently published in the literature [10], [11], [12], [13], [14], [15]. In [10], [11], [12], CRFID tags are designed using multi-resonators for encoding the desired information. Their EM signatures are measured using FD approach in which presence or absence of a resonance peak is noted. Similarly, in [13], multiple open-stub resonators are used to design a CRFID tag that works on FD technique. On the other hand, TD technique is used in [14], [15], in which delay-line structures encode data in their tags. Circuit-based CRFID tags can store large data, but their overall size and presence of transceiver module makes them complex and costly to manufacture.

A fully passive chipless tag that works on FD technique can further be categorized as: 1) retransmission-based and 2) RCS-based. Retransmission-based tags consist of RF circuits for encoding their data and antennas for sending and receiving EM signatures. The read range of such tags is long; however, they have comparatively large footprint [16], [17]. In comparison to retransmission-based tags, the RCS-based tags do not contain any antenna module for transmission and reception of the data. Therefore, the overall size of these tags is reduced, and consequently they have lower cost and complexity. This also leads to high code densities, which depends upon the physical configuration and size of the tag in question. The EM signatures of these tags are measured as radar cross section (RCS) and EM resonances present in the RCS are used to decode the encoded information [18].

Various design methodologies are used to generate RCS resonances within a particular frequency band of operation of the chipless tag. Different encoding techniques are then used to further enhance the tag's data capacity. For example, in [19], C-shaped resonator tags with high spectral efficiency of 4.58 bits/GHz and very low code density of 2.86 bits/cm^2 were presented. Similarly, in [20], a tag with very low code density of 1.25 bits/cm^2 and high spectral efficiency of 5 bits/GHz but having a large tag size of 30 $\times$ 40 mm^2 was proposed. In [21], an impedance loaded circular ring resonator with very low code density of 2.63 bits/cm^2 is presented. Besides these, there are a variety of tags that exploit dual-polarization feature to enhance the coding capacity. Such

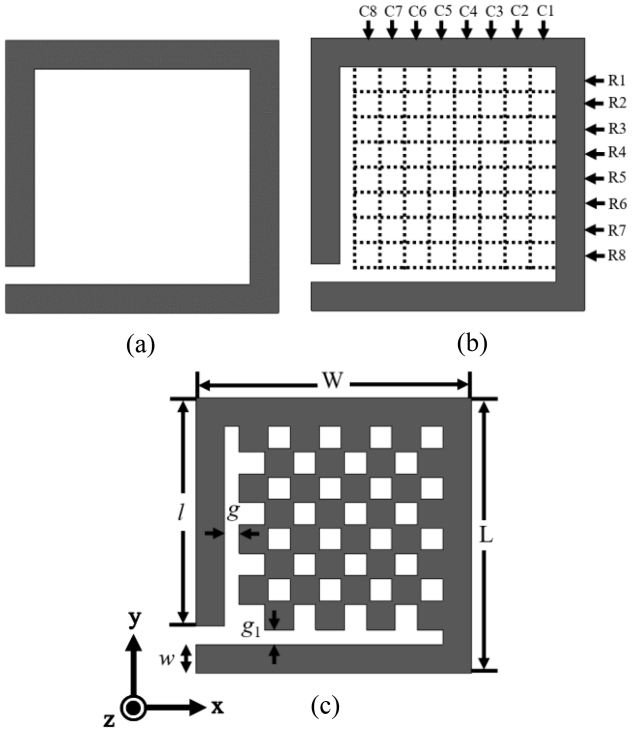

FIGURE 1. Chipless tag (a) Open-loop resonator. (b) Equally distributed into small cells. (c) Geometry of the checkerboard loaded open-loop resonator.

techniques include nested concentric square loop resonators [22] and L-shaped resonators [23] with large code density of 9.45 bits/cm^2 and 12 bits/cm^2 respectively. A stepped impedance resonator with very low code density of 1.06 bits/cm^2 having a large size of 30 $\times$ 25 mm^2 is proposed in [24]. A miniaturized open-loop resonator-based tag with size of 6.6 $\times$ 10.8 mm^2 achieves a high code density of 4.99 bits/cm^2 using very complex optimization technique is discussed in [25]. In [26], a tag with high spectral efficiency of 7 bits/GHz but low code density of 0.88 bits/cm^2 using non-iterative technique is presented. There are also other recently reported RCS-based tag structures like: L-shaped slot resonator [27], trefoil shaped slot resonator [28] and comb-shaped tag [29].

There is a great focus of the research community to reduce the overall size of a chipless tag achieving a highly miniaturized design with high code density through designing a compact resonating element. The researchers have employed different types of resonators as discussed above. Recently, an open-loop resonator using fragment loading technique to design a miniaturized tag applying a very complex genetic optimization algorithm is proposed [25]. The loading of a basic open loop provides a novel approach to reduce the overall footprint of a tag. Four distinct advantages can be expected by using loading technique to design any kind of loaded resonator. First, the empty area of different loop structures can be divided into small cells. Second, by using the empty area of a loop the overall size of the resonators can be reduced. Third,

TABLE 1. Optimized Parameters

Parameter	l	w	g	g_1	L	W
Value (mm)	3.15	0.4	0.2	0.2	3.8	3.8

loading with micro-metallic-cells (MMC) gives great flexibility to control the resonance frequency. Forth, using the loading technique to design checkerboard type structures gives a high level of security against counterfeiting because it is difficult to duplicate these types of structures [30]. Therefore, the loading technique to design checkerboard type resonators has the potential to reduce the overall resonator size resulting in a miniaturized tag with high code density compared to the conventional types of resonators. There are also several open-loop fragments loaded resonating structures presented in the literature [31], [32], [33], [34], [35], [36].

In this research, a novel design methodology for frequency-domain RCS-based chipless tags is presented. A square open-loop resonator of size 3.8 × 3.8 mm^2 is selected for designing a miniaturized tag. For multi-peak RCS resonances, a new kind of sequential loading approach is used that provides a great amount of flexibility. This new technique is simple but very effective resulting in checkerboard type resonators. These resonators are printed on front as well as on backside of a substrate for maximum data storage. The proposed tag achieves a very high code density of 10.94 bits/cm^2 and spectral efficiency of 2 bits/GHz while utilizing a frequency band from 6.5-10.5 GHz.

II. TAG DESIGN

The design approach of the proposed chipless tag will be presented in this section. First the geometric model and the design evolution will be explained, followed by its optimization.

A. MODELING OF CHECKERBOARD TAG BY LOADING THE OPEN-LOOP RESONATOR

The proposed tag is modelled on Rogers RT6035HTC substrate having thickness t = 0.762 mm, permittivity $\varepsilon_r = 3.5$ and loss tangent tan$\delta = 0.0013$. The proposed tag design is based on a miniaturized square open-loop resonators. Normally, the size of a tag must be small to achieve high bit capacity. To achieve this objective, a unique loading strategy is applied in which open-loop resonator is filled with small square metallic cells. The proposed design process is depicted in Fig. 1. The design starts with a square open-loop resonator, as shown in Fig. 1(a). The empty area inside the open-loop resonator is equally divided into small square cells as shown in Fig. 1(b). Lastly, a checkerboard structure is constructed by filling some of the cells with copper metal. The overall final resonator geometry is shown in Fig. 1(c). Each square has a dimension of 0.4 × 0.4 mm^2. There is no metallic ground plan on the backside of the final resonator substrate. The optimized parameters of open-loop checkerboard resonator design are listed in Table 1.

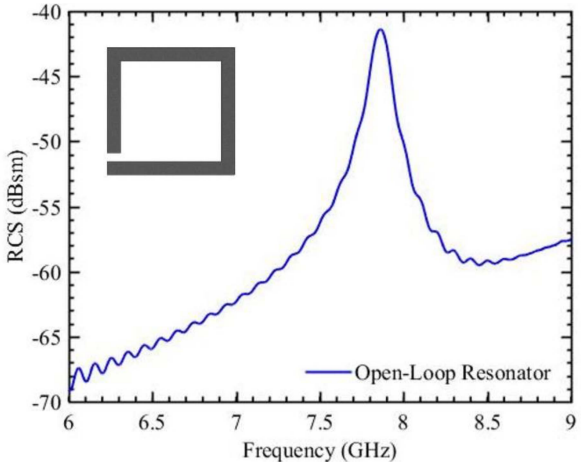

FIGURE 2. Layout and simulated RCS response of open-loop resonator versus frequency.

The performance of this checkboard resonator is analyzed in different steps using full-wave analysis in CST Microwave Studio. First, a single open-loop resonator with no loading will be analyzed. The length of the resonator is inversely proportional to its resonance frequency. An overall dimension of 4.2 × 4.2 mm^2 is chosen so that the resonator resonates at the desired lowest frequency of interest 7.86 GHz. The simulated RCS response is shown in Fig. 2.

The empty area inside the open-loop resonator is then equally distributed into 64 small cells with 8 rows from R1 to R8 and 8 columns from C1 to C8. Starting from the first column and first row (C1, R1) of the open-loop resonator and moving towards left, the alternating cells are filled (i.e., loaded) with metal. When the loading of first row is complete, the second row is started in a similar fashion but in an inverse manner. By sequentially loading the open-loop resonator, several new open-loop checkerboard resonators are constructed. This step-by-step development in the loading of the open-loop resonator is shown in Fig. 3(a)–(d).

As the empty area of the open-loop resonator becomes more loaded, the resonance-peak shifts towards higher frequencies. Hence, with the same overall dimension of the open-loop resonator, different new open-loop resonators can be constructed which resonate at different frequencies. This is done by simply loading the empty area of the open-loop resonator with small square metallic cells (see Fig. 1(c)).

B. OPTIMIZATION OF CHECKERBOARD OPEN-LOOP RESONATOR

The loading approach used in this paper provides great flexibility in designing RCS-based chipless tags as compared to the conventional design techniques. As discussed earlier, a square open-loop resonator is setup to provide a resonance peak at any desired operating frequency. The decision on the amount of loading each resonator with metallic cells is made by carefully analyzing the frequency shift in the RCS

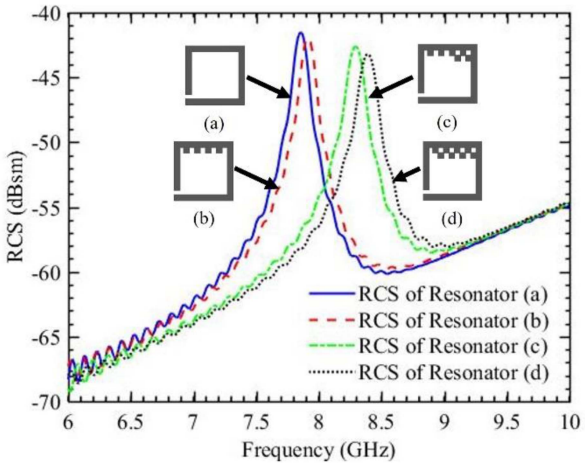

FIGURE 3. Progressive-loading of open-loop resonator and corresponding RCS-response vs. frequency. [Resonance-peaks of the respective configurations: (a) 7.86 GHz. (b) 7.91 GHz. (c) 8.29GHz. (d) 8.38 GHz].

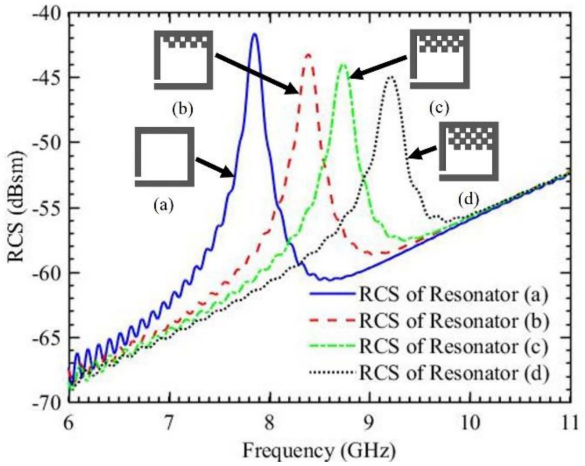

FIGURE 4. The optimized configurations of open-loop resonators and their RCS-response vs. frequency. [Resonance-peaks of respective tags: (a) 7.86 GHz. (b) 8.38 GHz. (c) 8.73 GHz. (d) 9.21 GHz].

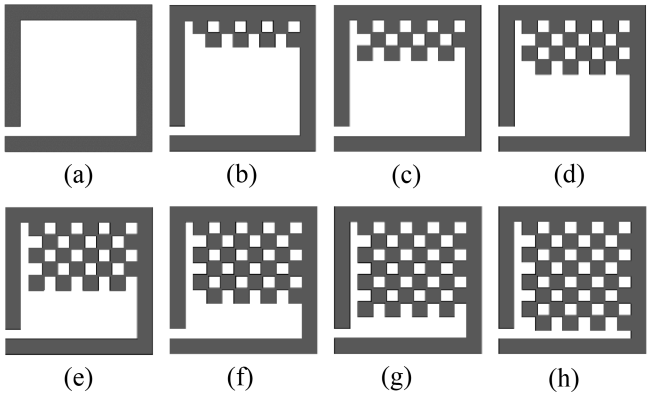

FIGURE 5. Eight different layouts after proper loading of open-loop square resonator. [Resonance-peaks of the respective tags: (a) 7.86 GHz. (b) 8.38 GHz. (c) 8.73 GHz. (d) 9.21 GHz. (e) 9.5 GHz. (f) 10.06 GHz. (g) 10.37 GHz. (h) 11.11 GHz.

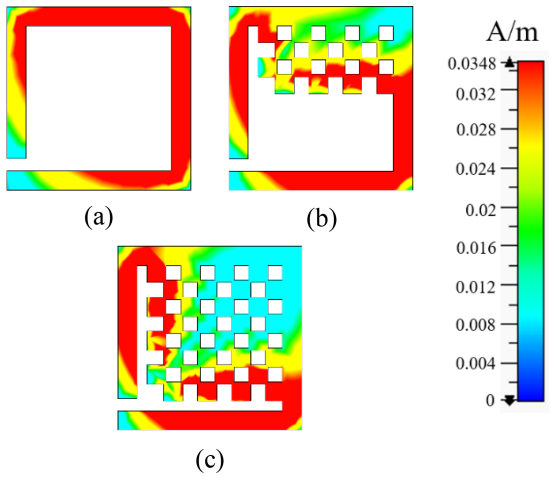

FIGURE 6. Surface current distribution of three different configurations at (a) 7.86 GHz (b) 9.21 GHz (c) 11.11 GHz.

response. For an efficient multi-peak RCS with high bit capacities, the resonances should be separated from each other by a significant guard band. In Fig. 3, it can be observed that when the open-loop resonator is loaded only with a single row, the resonances (as shown in case of (a) and (b), Fig. (3)) are very near to each other and can't be distinguish properly. However, the resonance peaks become significantly apart from each other if loading is achieved up to one and a half row as shown in Fig. 3(c). Hence based on this methodology and after parametric analysis, the optimized layouts of the tag loadings and corresponding RCS responses are shown in Fig. 4.

It is clear from Fig. 4, that by simply loading the open loop resonator with correct amount, several useful frequency resonators can be developed. As a proof of concept, seven different resonators with different RCS responses were achieved after proper loading and are shown in Fig. 5. A total of eight different resonators including the basic one, have thus been obtained.

To get an insight into the physics of the tag loading and its functioning, surface current distributions for three resonators are shown in Fig. 6. The surface current density for unloaded open-loop resonator when illuminated by a linearly polarized plane wave is depicted in Fig. 6(a). Similarly, currents for half-loaded and fully loaded resonators are shown in Fig. 6(b) and (c) respectively. It can be clearly observed that as the loading increases, the length of the current path decreases energizing the higher-order modes. The maximum current stays along the edges of the resonators, while the inner most part of the metallic cells are almost void of current resulting in resonance shift towards higher frequencies, this is in accordance with the frequency response depicted in Figs. 3 and 4.

III. CONFIGURATION SETTING OF CHECKERBOARD OPEN LOOP RESONATORS TO FORM TAGS

Once different layouts of loaded resonators were achieved such as those shown in Fig. 5, final tags can be realized using

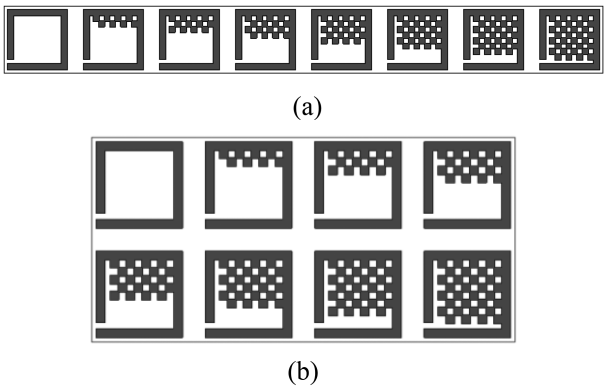

FIGURE 7. Two different configuration using loaded-open-loop resonators on front side of the substrate only. (a) Configuration-1 (1 × 8) and (b) Configuration-2 (2 × 4).

different arrangements of these layouts of loaded resonators. In this research, the authors, as a proof of concept, have chosen three different arrangements to achieve an optimum tag configuration.

In first arrangement, all resonators shown in Fig. 5 are placed in a single row forming a 1 × 8 matrix. The resonators are placed on the front side of the substrate only, thus resulting in an overall size of 37.8 × 4.2 mm^2. In the second arrangement, the eight resonators are placed in the form of two rows with 4 resonators each (i.e., 2 × 4 matrix). This reduces the length of the tag but increases its width. The overall size of this configuration is 18.6 × 9 mm^2, and hence the net tag area remains the same as that of the previous configuration. Both configurations (1 & 2) are shown in Fig. 7.

These configurations however are formed such that the resonators are printed on one side of the substrate. This is also a traditional way of making RFID tags. In this research, a new approach is used to reduce the tag size by a significant amount. In the next configuration, four of the bottom resonators of configuration-2 are moved onto the backside of the substrate. These backside resonators are subject to two transformations; first, each resonator is mirrored (i.e., flipped horizontally) and then rotated by 90° clockwise. These transformations are made to break the symmetry of the resonators on both sides of the substrate. The result is that maximum area of each resonator on the backside gets exposed to the incident plane wave. This has a drastic effect on the overall RCS response of the tag. This configuration also leads to a reduction in the overall footprint of the tag by half. This new configuration (i.e., Configuration-3) is shown in Fig. 8. In the third configuration, a single row of resonators on both front and backside of the substrate are laid out in 1 × 4 matrix form. This gives an overall tag size of 18.6 × 4.2 mm^2.

The RCS response of all configurations (1, 2 & 3) is shown in Fig. 9. It can be observed that for configuration 1 and 2, the RCS response has resonances with low RCS magnitude level that must be difficult to identify. On the other hand, the RCS response of configuration-3 contain resonances that are well apart and have very high RCS magnitude level

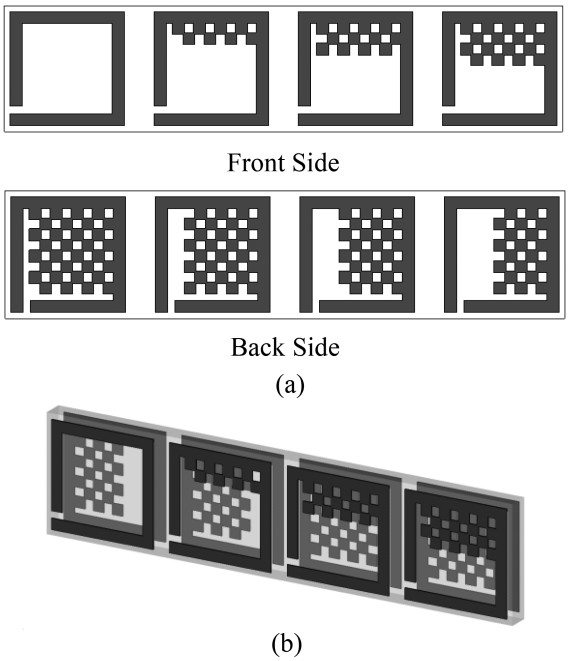

FIGURE 8. 3rd configuration using loaded-open-loop resonators on both front and back side of the substrate. (a) Plane view (b) Perspective view.

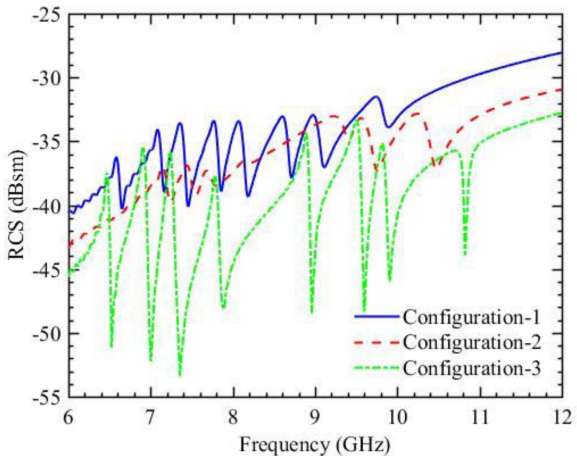

FIGURE 9. Simulated RCS response of configuration (1, 2 & 3).

that are easily distinguishable and detectable. Hence, the best choice for efficient performance will be configuration-3. The tag with configuration-3 is responsible for generating eight resonance peaks at distinct frequencies from 6.5 to 10.5 GHz. The RCS response of this tag is shown separately again in Fig. 10 for more clarity.

A. EFFECT OF INTER-RESONATOR SEPARATION

The spacing between the resonators affects both tag size as well as its RCS response. The spacing should be such that a best compromise between the tag size and an easily identifiable RCS signature must be reached out. The reduction in inter-resonator separation will increase mutual coupling thus

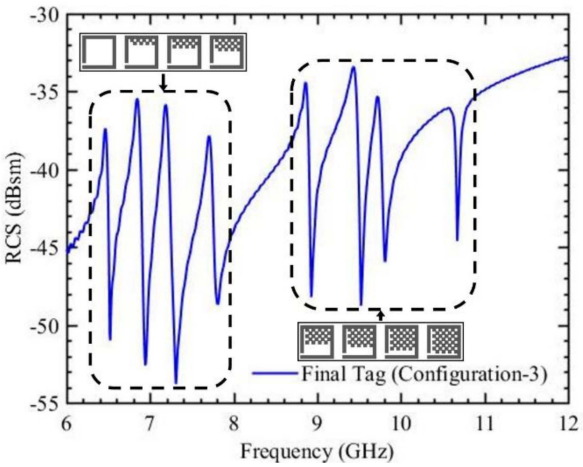

FIGURE 10. Simulated RCS response of final proposed CRFID tag.

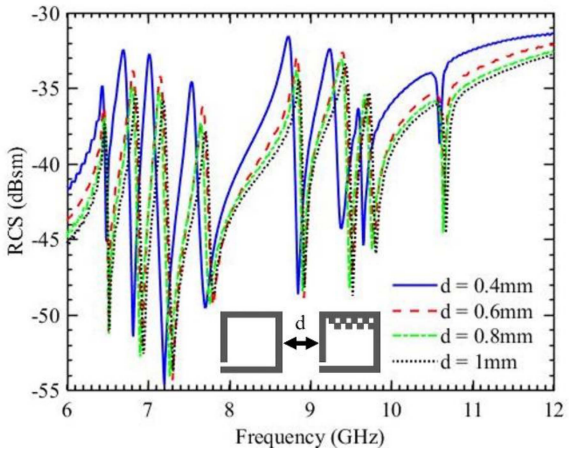

FIGURE 11. Effect of inter-resonator separation on RCS response of tag.

resulting in a frequency shift of RCS response. The spacing "d" between the resonators is kept at 1 mm for all the three configurations (1-3). A parametric study, however, for various separation distances "d" versus RSC resonances is done and shown in Fig. 11. It has been observed that reducing "d" shifts the RCS towards lower frequencies. The minimum possible value of "d" for which the RCS remains stable is 0.4 mm. Further reduction in "d" results RCS goes out of the operating band. The optimum value of d = 0.6 mm was chosen for the proposed design. This final value of d updated the overall size of the proposed tag to 17.4×4.2 mm^2.

B. EFFECT OF SUBSTRATE THICKNESS

The effect of variation in substrate thickness on RCS response of the tag is shown in Fig. 12. The effect of substrate thickness is three folds. 1) Efficient utilization of the spectrum: It can be observed from Fig. 12 that for thinner substrates the spectrum efficiency of the tag is lower as compared to thicker substrates. The RCS response for t = 0.762, and t = 1 mm has the best efficiencies. 2) Identification of upper and lower nibble: As discussed earlier, in this paper a unique configuration of

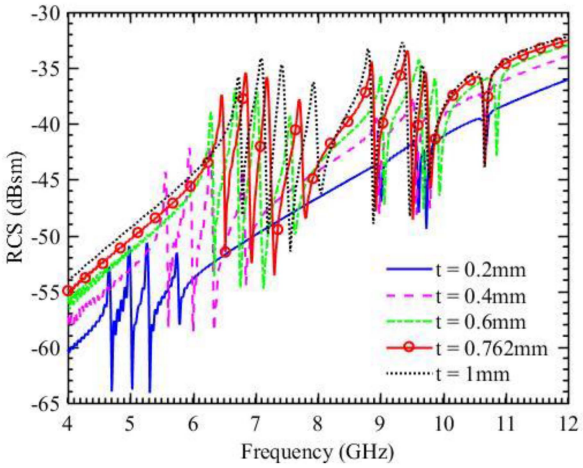

FIGURE 12. Effect of substrate thickness on RCS response of tag.

resonator's layout is proposed. Based on this proposed layout, it would be useful if the reader (i.e., CRFID tag reader) could also distinguish between the responses of resonators at the back and on the front sides. That is to say, that upper and lower nibbles of the "Single Byte" should be distinguishable. This has been referred to pictorially by dotted lines in Fig. 10. Setting this criterion of intelligent use of the layout, it can be keenly observed in Fig. 12 that the upper and lower nibbles in RCS response of the tag with t = 0.762 mm is better separated than that for the tag with t = 1 mm. 3) RCS amplitude: The choice of substrate thickness is also based on the fact that for thinner substrates, the RCS magnitudes are lower. In general, RCS magnitudes of lower values should be avoided as they may result in poor detection of tags ID. The optimum substrate thickness based on the analysis shown in Fig. 12 is 0.762 mm.

C. ILLUMINATION OF TAG FROM FRONT AND BACK SIDES

The proposed tag is unique in its construction as it is comprised of resonators on both sides of the substrate. Therefore, it was interesting to show whether this tag would perform well when illuminated from either side. The results are shown in Fig. 13, whereby the RCS response of the tag put in either way facing towards the reader is shown. It can be stated with quite confidence that the RCS response remains the same for both the cases. Therefore, the proposed tag is orientation independent and can be used in a horizontally flipped mode as well.

IV. MEASUREMENT RESULTS

The tags were fabricated using standard PCB process. The photographs of the fabricated prototypes are shown in Fig. 14. The measurements of these tags were carried out inside an anechoic chamber in a bi-static configuration. The configuration setup and photograph of the measurement setup is shown in Fig. 15.

The two horn antennas placed side by side, were used for transmission and reception of electromagnetic (EM) waves. The horn antennas were connected to vector network analyzer

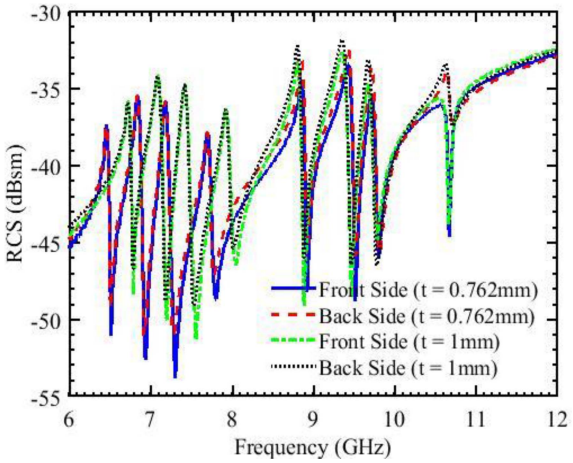

FIGURE 13. RCS response of proposed tag when illuminated from either front or back side.

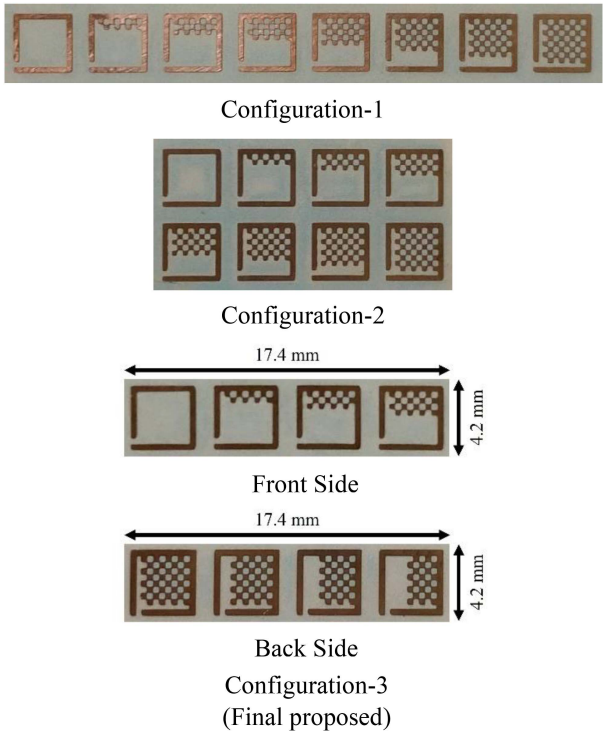

FIGURE 14. Photographs of the fabricated CRFID tag prototypes.

E8362B. The gain of horn antennas used was 12 dBi while the power delivered by the VNA to them was set to 7 dBm. The complex S_{21} parameter of the tag is measured by using the above mentioned bi-static configuration in an anechoic chamber. The signal received from the tag at port 2 of VNA was very week, therefore an isolation measurement without the tag was also performed. This is an important step to remove any static noise. The effects due to horn antennas were also considered by measuring S_{21} of a reference rectangular metallic plate with a known RCS. Finally, the RCS response of the proposed tag was calculated by using following formulation

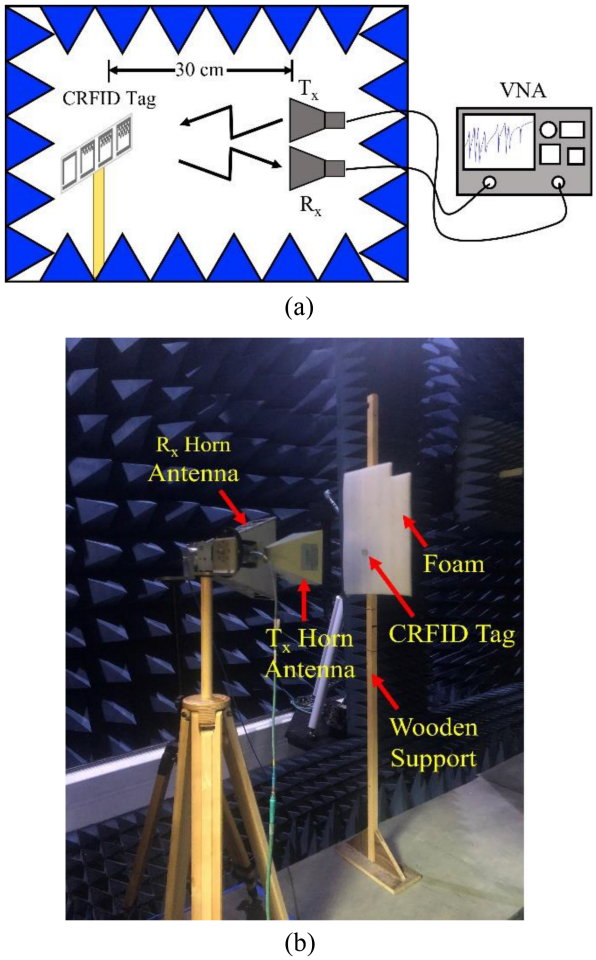

FIGURE 15. Measurement setup: (a) block diagram of the bi-static configuration used (b) Panoramic photograph of RCS measurement setup inside an anechoic chamber.

(1) [19].

$$\sigma^{\text{tag}} = \left[\frac{S_{21}^{\text{tag}} - S_{21}^{\text{isolation}}}{S_{21}^{\text{ref}} - S_{21}^{\text{isolation}}}\right]^2 \cdot \sigma^{\text{ref}} \tag{1}$$

Where, S_{21}^{tag} and S_{21}^{ref} is the measured S-parameter of the proposed tag and reference rectangular metallic plate, respectively. The $S_{21}^{\text{isolation}}$ is isolation measurement without the tag, σ^{ref} is a known RCS value of the reference metallic plate and σ^{tag} is RCS value of the proposed CRFID tag.

The prototype CRFID tag was attached to a foam. Therefore, the measured response contained effects from foam as well. The foam only response was thus measured as well. This extra foam effect was subtracted from the tag response. The measured RCS response of final proposed tag (Configurations-3) along with original simulated RCS response is shown in Fig. 16. The measured results of configuration-3 agree quite well with those of simulated RCS response.

Applying the given approach, a resonator layout can be designed with different bit capacities. However, to maintain

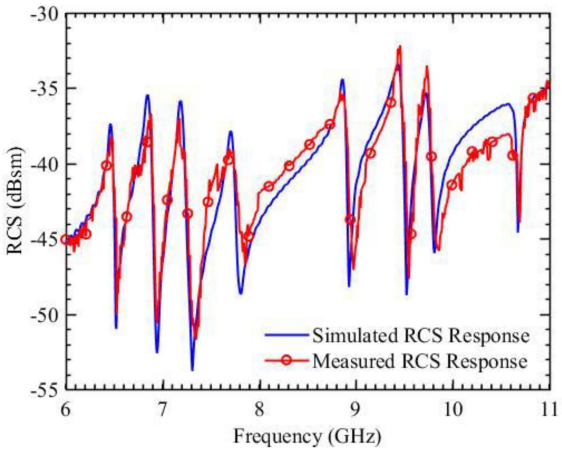

FIGURE 16. Measured and Simulated RCS Response of Final Proposed Tag (Configuration-3).

TABLE 2. Comparison With State-of-the-Art CRFID Tags

Ref. No.	Operating Frequency (GHz)	Tag Size (mm^2)	Bits Per Resonator	Code Density ($bits/cm^2$)	Spectral Efficiency (bits/GHz)
[19]	2.5–7.5	20 × 40	4.58	2.86	4.58
[20]	2–5	30 × 40	3	1.25	5
[21]	3–9	30 × 30	3	2.63	3.95
[22]	8–14	13.8 × 13.8	2.25	9.45	3
[23]	4.8–10	15 × 10	2	12	3.46
[24]	3.1–10.6	30 × 25	2	1.06	1.06
[25]	2.8–6	6.6 ×10.8	3.56	4.99	1.11
[26]	1.7–4.7	66 × 36	3	0.88	7
[27]	3–6	20 × 20	1	4	5.33
[28]	5.4–10.4	13.55 × 13.55	1	5.44	2
[29]	4.5–7.5	17 × 14	1	5.88	4.66
Proposed Tag	6.5–10.5	17.4 × 4.2	1	10.94	2

simplicity, the proposed resonator has been assigned single bit. The tag is then an 8-bit tag and can store up-to one BYTE of information. The frequency span of the tag operation is 6.5-10.5 GHz with physical area of $17.4 \times 4.2 = 73.08$ $mm^2 = 0.7308$ cm^2. Therefore, the tag has code density of 10.94 $bits/cm^2$ and a spectral efficiency of 2 bits/GHz. The final proposed CRFID tag is compared with state-of-the-art published work in Table 2. The code density of the proposed tag is comparatively very high among the designs presented in the Table. Moreover, the bit capacity can be doubled if frequency shift coding (FSC) is used. A single resonator can be assigned two bits (one for the high value, the other for the lower value of the resonance) hence doubling the bit-capacity to 16-bits.

V. CONCLUSION

A unique and novel methodology to structure a chipless tag was presented. The tag consisted of a square open-loop resonator that was gradually loaded with small metallic cells. The methodology presented is simple and can achieve EM signature of various bit-lengths with a considerable ease. The tag capacity was further enhanced by proposing a double-side layout of resonators. The overall geometry of the tag's individual resonators resembles a checkerboard. The overall size of the tag obtained was 17.4×4.2 mm^2, which is very compact. The band of operation for the proposed tag is 6.5-10.5 GHz. These numbers result in an efficient chipless tag that has a high code density of 10.94 $bits/cm^2$ and spectral efficiency of 2 bits/GHz. The tag design methodology proposed in this paper is quite simple but very powerful. This unique tag can therefore be used in a wide range of modern identification scenarios.

REFERENCES

[1] H. Shan, J. Peterson III, S. Hathorn, and S. Mohammadi, "The RFID connection: RFID technology for sensing and the Internet of Things," *IEEE Microw. Mag.*, vol. 19, no. 7, pp. 63–79, Nov./Dec. 2018.

[2] A. Lozano-Nieto, "Basic principles of radiofrequency identification," in *RFID Design Fundamentals Applications*. Boca Raton, FL, USA: Taylor Francis, 2010, pp. 5–6.

[3] N. C. Karmakar, E. M. Amin, and J. K. Saha, *Chipless RFID Sensors*. Hoboken, NJ, USA: Wiley, 2016.

[4] S. Dey, J. K. Saha, and N. C. Karmakar, "Smart sensing: Chipless RFID solutions for the Internet of everything," *IEEE Microw. Mag.*, vol. 16, no. 10, pp. 26–39, Nov. 2015.

[5] S. Preradovic and N. C. Karmakar, "Chipless RFID: Bar code of the future," *IEEE Microw. Mag.*, vol. 11, no. 7, pp. 87–97, Dec. 2010.

[6] O. Boularess, H. Rmili, T. Aguili, and S. Tedjini, "Analysis of electromagnetic signature of Arabic alphabet as RF elementary coding particles," *Wireless Power Transfer*, vol. 2, pp. 97–106, 2015.

[7] L. M. Arjomandi, G. Khadka, Z. Xiong, N. C. Karmakar, and X. Zixang, "Document verification: A cloud-based computing pattern recognition approach to chipless RFID," *IEEE Access*, vol. 6, pp. 78007–78015, 2018.

[8] N. C. Karmakar, "Tag you're it radar cross section of chipless RFID tags," *IEEE Microw. Mag.*, vol. 17, no. 7, pp. 64–74, Jul. 2016.

[9] M. A. Islam and N. C. Karmakar, "Compact printable chipless RFID systems," *IEEE Trans. Microw. Theory Techn.*, vol. 63, no. 11, pp. 3785–3793, Nov. 2015.

[10] U. A. Haider, M. Noman, H. Ullah, and F. A. Tahir, "A compact L-shaped 16 bit polarization independent chipless RFID Tag," in *Proc. Int. Conf. U.K.-China Emerg. Technol.*, 2020, pp. 1–3.

[11] U. A. Haider, M. Noman, H. Ullah, and F. A. Tahir, "A compact chipless RFID tag for IoT applications," in *Proc. IEEE Int. Symp. Antennas Propag. North Amer. Radio Sci. Meeting*, 2020, pp. 1449–1450.

[12] M. Noman, U. A. Haider, H. Ullah, F. A. Tahir, H. Rmili, and A. I. Najam, "A 32-bit single quadrant angle-controlled chipless tag for radio frequency identification applications," *Sensors*, vol. 22, no. 7, 2022, Art. no. 2492.

[13] C. M. Nijas et al., "Chipless RFID tag using multiple microstrip open stub resonators," *IEEE Trans. Antennas Propag.*, vol. 60, no. 9, pp. 4429–4432, Sep. 2012.

[14] R. Bhattacharyya, C. Floerkemeier, and S. Sarma, "Towards tag antenna based sensing—An RFID displacement sensor," in *Proc. IEEE Int. Conf. RFID*, 2009, pp. 95–102.

[15] S. Shrestha, J. Vemagiri, M. Agarwal, and K. Varahramyan, "Transmission line reflection and delay-based ID generation scheme for RFID and other applications," *Int. J. Radio Freq. Identification Technol. Appl.*, vol. 1, no. 4, pp. 401–416, 2007.

[16] D. Betancourt, M. Barahona, K. Haase, G. Schmidt, A. Hübler, and F. Ellinger, "Design of printed chipless-RFID tags with QR-code appearance based on genetic algorithm," *IEEE Trans. Antennas Propag.*, vol. 65, no. 5, pp. 2190–2195, May 2017.

[17] M. A. Ashraf et al., "Design and analysis of multiresonators loaded broadband antipodal tapered slot antenna for chipless RFID applications," *IEEE Access*, vol. 5, pp. 25798–25807, 2017.
[18] M. Noman et al., "12-bit chip-less RFID tag with high coding capacity per unit area," in *Proc. IEEE Int. Symp. Antennas Propag. USNC-URSI Radio Sci. Meeting*, 2022, pp. 127–128.
[19] A. Vena, E. Perret, and S. Tedjini, "Chipless RFID tag using hybrid coding technique," *IEEE Trans. Microw. Theory Techn.*, vol. 59, no. 12, pp. 3356–3364, Dec. 2011.
[20] O. Rance, R. Siragusa, P. Lemaître-Auger, and E. Perret, "Toward RCS magnitude level coding for chipless RFID," *IEEE Trans. Microw. Theory Techn.*, vol. 64, no. 7, pp. 2315–2325, Jul. 2016.
[21] Y. Ni et al., "Hybrid coding chipless tag based on impedance loading," *IET Microw. Antennas Propag.*, vol. 11, no. 10, pp. 1325–1331, 2017.
[22] H. Huang and L. Su, "A compact dual-polarized chipless RFID tag by using nested concentric square loops," *IEEE Antennas Wireless Propag. Lett.*, vol. 16, pp. 1036–1039, Oct. 2016.
[23] M. Noman, U. A. Haider, H. Ullah, A. M. Hashmi, and F. A. Tahir, "Realization of chipless RFID tags via systematic loading of square split ring with circular slots," *IEEE J. Radio Freq. Identification*, vol. 6, pp. 671–679, Oct. 2022.
[24] C. M. Nijas et al., "Low-cost multiple-bit encoded chipless RFID tag using stepped impedance resonator," *IEEE Trans. Antennas Propag.*, vol. 62, no. 9, pp. 4762–4770, Sep. 2014.
[25] L. Wang, T. Liu, J. Sidénn, and G. Wang, "Design of chipless RFID tag by using miniaturized open-loop resonators," *IEEE Trans. Antennas Propag.*, vol. 66, no. 2, pp. 618–626, Feb. 2018.
[26] Y. S. Chen, T. Y. Jiang, and F. P. Lai, "Automatic topology generation of 21 bit chipless radio frequency identification tags using a noniterative technique," *IEEE Antennas Wireless Propag. Lett.*, vol. 18, no. 2, pp. 293–297, Feb. 2019.
[27] V. Sharma, S. Malhotra, and D. M. Hashmi, "Slot resonator based novel orientation independent chipless RFID tag configurations," *IEEE Sensors J.*, vol. 19, no. 13, pp. 5153–5160, Jul. 2019.
[28] S. Tariq et al., "Orientation independent chipless RFID tag using novel trefoil resonators," *IEEE Access*, vol. 7, pp. 122398–122407, 2019.
[29] F. Babaeian and N. C. Karmakar, "Compact multi-band chipless RFID resonators for identification and authentication applications," *Electron. Lett.*, vol. 56, no. 14, pp. 724–727, Jul. 2020.
[30] Z. Ali et al., "Authentication using metallic inkjet-printed chipless RFID tags," *IEEE Trans. Antennas Propag.*, vol. 68, no. 5, pp. 4137–4142, May 2020.
[31] P. Mondal and M. K. Mandal, "Design of dual-band bandpass filters using stub-loaded open-loop resonators," *IEEE Trans. Microw. Theory Techn.*, vol. 56, no. 1, pp. 150–155, Jan. 2008.
[32] R. K. Maharjan and N.-Y. Kim, "Miniature stubs-loaded square open loop bandpass filter with asymmetrical feeders," *Microw. Opt. Technol. Lett.*, vol. 55, no. 2, pp. 329–332, Feb. 2013.
[33] A. Gorur, C. Karpuz, and M. Akpinar, "A reduced-size dual-mode bandpass filter with capacitively loaded open loop arms," *IEEE Microw. Wireless Compon. Lett.*, vol. 13, no. 9, pp. 385–387, Sep. 2003.
[34] R. Ghatak, M. Pal, P. Sarkar, and D. R. Poddar, "Dual-band bandpass filter using integrated open loop resonators with embedded ground slots," *Microw. Opt. Technol. Lett.*, vol. 54, no. 9, pp. 2049–2052, Sep. 2012.
[35] X. Y. Zhang, J.-X. Chen, and Q. Xue, "Compact bandpass filter using open-loop resonators with capacitive loading," *Microw. Opt. Technol. Lett.*, vol. 49, no. 1, pp. 83–84, Jan. 2007.
[36] Q. Zhao, G. Wang, and D. Ding, "Compact microstrip bandpass filter with fragment-loaded resonators," *Microw. Opt. Technol. Lett.*, vol. 56, no. 12, pp. 2896–2899, Dec. 2014.